1.6 Coupling of WRF and building-resolving urban CFD models for analysis of strong winds over an urban area

Hiromasa Nakayama[1]*, Tetsuya Takemi[2] and Haruyasu Nagai[1]

[1]Japan Atomic Energy Agency, Ibaraki, Japan

[2]Disaster Prevention Research Institute, Kyoto University, Kyoto, Japan

1. INTRODUCTION

The highly variable and complex phenomena of atmospheric flow are characterized by mainly two factors: large-scale meteorological disturbances and small-scale wind fluctuations produced by surface terrains and roughness elements. According to the observational study of Van der Hoven (1957), the spectrum of horizontal wind speed near the ground surface shows a large peak near period of 4days and a small peak near a period of 1 minute. The former is due to large-scale atmospheric motions and the latter is due to turbulence. Particularly, for densely built urban area covered with highly rough ground surface, high-rise buildings have significant influences on the small-scale fluctuations of atmospheric flow. In cases of strong winds induced by meteorological disturbances, the occurrence of gusty winds over such urban areas should be considered in terms of disaster prevention and urban planning.

For understanding the wind system over urban areas, a numerical modeling is a useful tool. To simulate and forecast atmospheric flows in real meteorological settings, numerical weather prediction (NWP) models are commonly used. Although the accuracy of NWP models for daily weather is continuously improving, it is difficult to reproduce small-scale fluctuations induced by urban roughness elements that are not explicitly represented in the NWP models.

For simulating wind flows accounting for the urban surface geometries, a computational fluid dynamics (CFD) technique is one of the commonly used approaches. In the CFD models, urban surface geometries can be explicitly represented at high resolutions. In particular, LES-based CFD model has been regarded as an effective tool with the rapid development of computational technology. LES model can reproduce small-scale wind fluctuations such as turbulent behaviors around obstacles. Therefore, an approach to couple the LES-based CFD and the NWP models should be promising to simulate strong winds over actual urban areas under real meteorological conditions.

In order to couple NWP and CFD models, the NWP outputs can be used as the initial and boundary conditions of a CFD model. Here, a serious issue is encountered when imposing unsteady turbulent inflow data for LESs from the NWP outputs, because the NWP models are not able to reproduce small-scale turbulent fluctuations. Therefore, a proper coupling technique should be applied, considering the generation of turbulent inflow for LESs.

To generate effectively turbulent inflows, the rescaling technique of Lund et al. (1998) is useful. They produced realistic turbulent fluctuations by rescaling the velocity field at a downstream station and re-introducing at the inlet in the special domain.

In this study, we extend the existing turbulent inflow technique to couple the CFD and NWP models. We conduct a building-resolving LES of strong winds over the central district of Tokyo during the passage of a major typhoon and examine the usefulness of our approach by comparing the LES results with the observations.

---

*Corresponding author address: Hiromasa Nakayama, Japan Atomic Energy Agency, Ibaraki, Japan; e-mail: nakayama.hiromasa@jaea.go.jp

2. NUMERICAL MODEL
2.2 MESOSCALE METEOLOROGICAL SIMULATION MODEL

The Weather Research and Forecasting (WRF) model, the Advanced Research WRF Version 3.1.1 (Skamarock et al. 2008) is used for a mesoscale meteorological simulation. We use a nesting capability to resolve the Tokyo region at a fine grid spacing by setting one-way nested, four computational domains (with the top being at the level of 50 hPa). The four domains cover areas of 1800 km by 1900 km at 4.5-km grid, 270 km by 300 km at 1.5-km grid, 93 km by 93 km at 300-m grid, and 25 km by 30 km at 60-m grid, respectively (Figs. 1a-1d). The number of vertical levels is 43, with 15 levels in the lowest 1-km depth.

The terrain data for the modeled topography are the global 30-second data (GTOPO30) from the U.S. Geological Survey for the outer 2 domains and the 50-m mesh digital elevation dataset by the Geographical Survey land-use and land cover

information is obtained from the 100-mesh dataset from the Ministry of Land, Infrastructure, Transport and Tourism of Japan.

As the initial and boundary conditions, we use 6-hourly Mesoscale Analysis (MANAL) data of Japan Meteorological Agency (JMA), 6-hourly Final Analysis data of the U.S. National Centers for Environmental Prediction, and daily Merged Sea Surface Temperature (MGDSST) analyses of JMA. The horizontal resolutions of MANAL and MGDSST are 10 km and 0.25 degree, respectively, which are useful for high-resolution mesoscale simulations.

Full physics processes are included in the present simulation in order to reproduce real meteorological phenomena. A physics parameterization that is closely relevant to the simulation of wind fields is a PBL mixing parameterization. We choose a Mellor-Yamada Level 2.5 scheme of Janjic (2002) in which the used only for the outermost domain, and a vertical
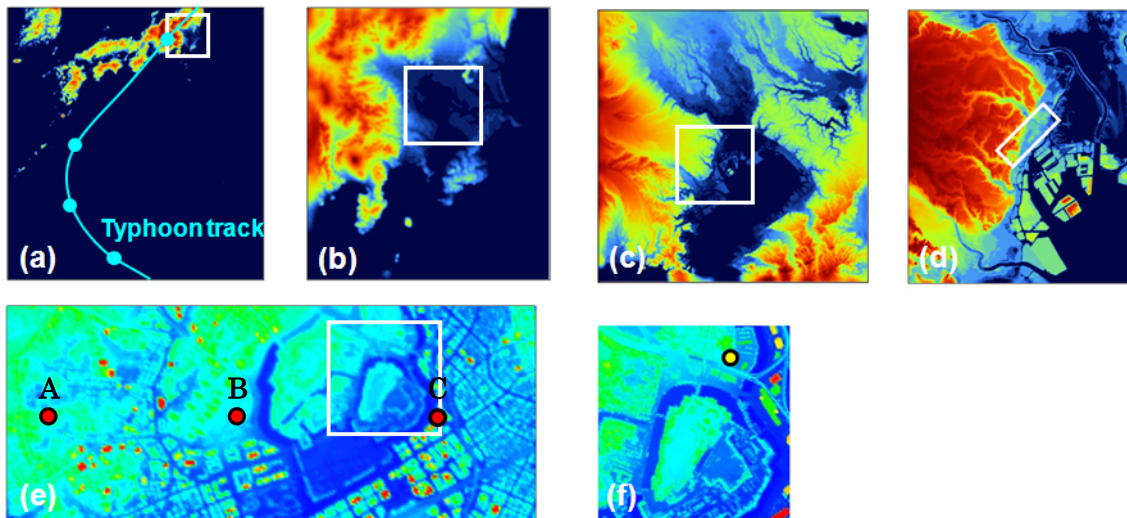
Figure 1: Computational areas of the nested WRF models for (a) the 4.5-km grid, (b) the 1.5-km grid, (c), the 300-m grid, and (d) the 60-m grid domains and of the CFD models for (e) the 20-m grid and (f) the 5-m grid. The inflow boundary of the CFD model is on the left. The color shading in (a)-(d) indicates the surface elevation scaled by the maximum height in each domain (2409 m in (a); 3285 m in (b); 255 m in (c); and 54 m in (d)). The white rectangular in (a)-(d) indicates the area of the child domain. The color shading in (e) and (f) indicates the height of the buildings and structures. The points A, B, and C in (e) represent the locations used in Fig. 2. The yellow circle in (f) indicates the locations of the wind observation site in Fig. 3.

levels. A Kain-Fritch cumulus scheme is warm-rain and ice-phase microphysics scheme is employed for cloud and precipitation processes in all the domains.

The case studied here is a high-wind event in Tokyo during the passage of Typhoon Melor (2009) that attained the central pressure of 910 hPa and the maximum 10-min averaged wind of 55 m s^{-1} at its maximum intensity on 4 October 2009 and made landfall on the Japan coast about 280 km west of Tokyo at around 2000 UTC 7 October. The maximum instantaneous wind speed recorded in Tokyo was 30.2 m s^{-1} at 2339 UTC 7 October. In order to simulate wind fields for this event, the computation for the outermost domain is initialized at 0000 UTC 6 October 2009, while the simulations for the 2 innermost domains are initialized at 1800 UTC 7 October. The simulated outputs of the innermost domain at 1-min interval are used as the inputs of a CFD model.

2.2 LES-BASED CFD MODEL

The CFD model is based on the LES model developed by Nakayama et al. (2011). The governing equations are the filtered continuity equation and the filtered Navier-Stokes equation, as follows:

$$\frac{\partial \overline{u}_i}{\partial x_i} = 0, \tag{1}$$

$$\frac{\partial \overline{u}_i}{\partial t} + \overline{u}_j \frac{\partial \overline{u}_i}{\partial x_j} = -\frac{1}{\rho}\frac{\partial \overline{p}}{\partial x_i} + \frac{\partial}{\partial x_j}\nu\left(\frac{\partial \overline{u}_i}{\partial x_j} + \frac{\partial \overline{u}_j}{\partial x_i}\right) - \frac{\partial}{\partial x_j}\tau_{ij} + f_i \tag{2}$$

$$\tau_{ij} = \overline{u_i u_j} - \overline{u}_i \overline{u}_j \tag{3}$$

$$\tau_{ij} - \frac{1}{3}\delta_{ij}\tau_{kk} = -\nu_{SGS}\overline{S}_{ij} \quad \nu_{SGS} = \left(C_s f_s \overline{\Delta}\right)^2 \left(2\overline{S}_{ij}\overline{S}_{ij}\right)^{\frac{1}{2}} \tag{4}$$

$$\overline{S}_{ij} = \left(\partial\overline{u}_i/\partial x_j + \partial\overline{u}_j/\partial x_i\right)/2 \tag{5}$$

and

$$\overline{\Delta} = \left(\overline{\Delta}_x \overline{\Delta}_y \overline{\Delta}_z\right)^{\frac{1}{3}} \tag{6}$$

where $u_i, t, p, \rho, \tau_{ij}, \delta_{ij}, \nu, \nu_{SGS},$ and u^* are wind velocity, time, pressure, density, subgrid-scale Reynolds stress, Kronecker delta, kinematic

viscosity, eddy viscosity coefficient, and friction velocity, respectively. Subscript i and j stand for coordinates (streamwise direction: $x_1 = x$, spanwise: $x_2 = y$, and vertical: $x_3 = z$). Variables with an upper bar denote spatially filtered ones. In this study, the standard Smagorinsky model (Smagorinsky 1963) is employed because of its simplicity and low computational cost. C_s is set to 0.1. f_s is the Van Driest damping function (Van Driest 1956). $\overline{\Delta}$ denotes grid-filter width. The body force, f_i, is included in the Navier-Stokes equations in order to incorporate the effects of buildings on fluid flow. The feedback forcing formulation by Goldstein et al. (1993) is used to represent this body force and is expressed as follows:

$$f_i = \alpha \int_0^t u_i(t')dt' + \beta u_i(t), \quad \alpha < 0, \beta < 0 \tag{7}$$

where α and β are negative constants. The stability limit is given by $\Delta t < \dfrac{-\beta - \sqrt{(\beta^2 - 2\alpha k)}}{\alpha}$ and k is a constant value of order 1.

The buildings in the central district of Tokyo are explicitly represented by a digital surface model dataset at 2-m resolution. Two computational domains are used. The size of the domain (e) where the urban surface geometry is explicitly resolved is 5.0 km (streamwise) by 2.0 km (spanwise) with the depth of 1.5 km (Fig. 1e), with buffer zones with a 500-m length being placed at the up- and down-stream of the building-resolved area. Thus, the length of the main analysis domain is 6.0 km. The total mesh number is 300 by 100 by 80 nodes. The grid spacing is 20 m in the horizontal directions and 2.5-64 m stretched in the vertical direction. The size of the domain (f) where the individual urban buildings are explicitly resolved is 1.0 km (streamwise) by 1.0 km (spanwise) with the depth of 1.5 km (Fig. 1f), with buffer zones with a 500-m length being placed at the up- and down-stream of the building-resolved area. Thus, the length of the main analysis domain

is 3.0 km. The total mesh number is 300 by 200 by 80 nodes. The grid spacing is 5-m in the horizontal directions. The grid spacing in the vertical direction is the same as the one in the LES model domain (e).

The coupling algorithm of the velocity and pressure fields is based on the MAC method (Chorin 1967) with the Adams-Bashforth scheme for time integration. The time step interval is 0.05 second. The Poisson equation is solved by the SOR method. For the spatial discretization, a second-order-accurate central difference is used.

The boundary conditions without applying the WRF outputs are: a Sommerfeld radiation condition (Gresho 1992) at the outflow boundary; a free-slip condition for the horizontal velocity components and zero-speed condition for the vertical velocity component at the upper boundary; a no-slip condition for each velocity component at the bottom surface; and a periodic condition at the spanwise lateral boundaries.

On the other hand, the inflow boundary condition of the LES model domain (e) is determined by the temporally and spatially varying wind components interpolated on the LES resolutions from the WRF model outputs at 1-min interval and 60-m grid spacing. The inflow boundary condition of the CFD model domain (f) is determined by the temporally and spatially varying wind components interpolated on the LES resolutions from the CFD model (e) outputs at 0.05-sec interval and 20-m grid spacing.

2.3 COUPLING WRF AND URBAN CFD MODELS

The WRF model cannot reproduce turbulent fluctuations because the individual urban buildings and obstacles are not explicitly resolved. To ingest the WRF outputs for a building-resolving LES, turbulent fluctuations induced by urban roughness elements should be added to the WRF wind flows. The rescaling approach of Lund et al. (1998) is considered to be useful in terms of both saving computational resources and physical consistency to boundary-layer dynamics. However, this technique is not appropriate to simulate atmospheric flows under real meteorological conditions because the mean flow actually changes with time owing to the meteorological variations. Therefore, we extend the method of Lund et al. by taking into account the temporal and spatial variations of the mean flow at the inflow boundary of the LES model. The WRF outputs during 2300 UTC 7 October and 0000 UTC 8 October are used for the present LES.

3. RESULTS

The simulated central pressure just before the landfall at around 2000 UTC 7 October was 953 hPa, which well agrees with the corresponding best-track value of 955 hPa. In addition, the observed track of Typhoon Melor (2009) was well reproduced in the outermost domain of the WRF model. Thus, the WRF model is considered to successfully simulate the track and intensity of Typhoon Melor (2009) before and during the landfall on 7 October 2009, which indicates that the WRF outputs for use in the present LES reflect the overall features of the strong winds induced by the typhoon.

Figure 2 the streamwise variation of the vertical profiles of wind speeds from the WRF and the LES models. The points A, B, and C are located at 1.0 km, 2.7 km, and 4.6 km distances downstream of the upstream boundary the main analysis domain (Fig. 1e). The LES winds seem to fluctuate around the WRF winds above about the 100-m height. Below the 100-m height, the LES winds become significantly weaker than the WRF winds. These decrease of wind speeds are clearly induced by resolving the urban surface geometries in the LES model. Furthermore, the turbulent fluctuations in the LES are well represented at each downstream position. This fact indicates that the present approach is effective in producing urban boundary layer flow.
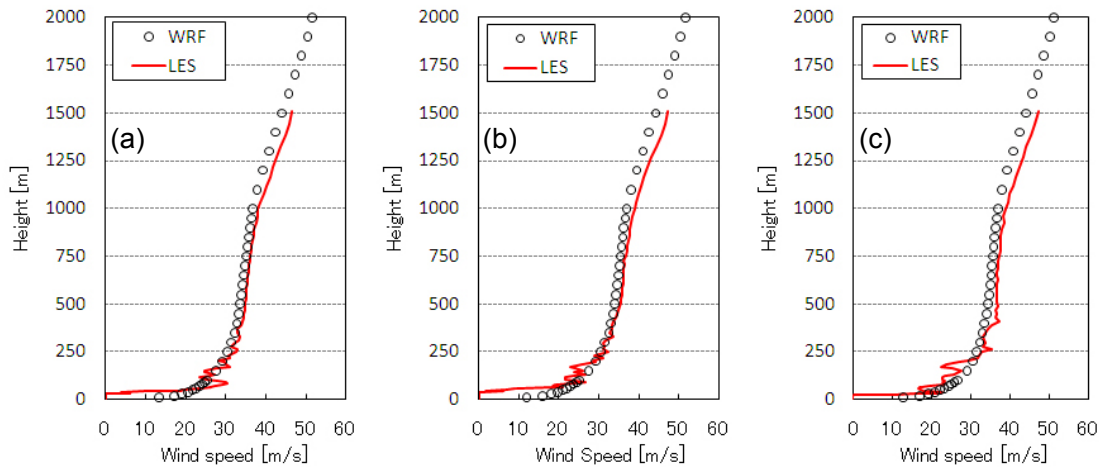
Figure 2: The vertical profiles of wind speeds from the WRF (circles) and the LES (solid line) models at the points (a) A, (b) B, and (c) C (see Fig. 1e) at 0000 UTC 8 October 2009.

Figure 3 compares the time series of 10-minute averaged wind speed obtained at the JMA observation site (see Fig. 1f) and the simulated wind speed at the corresponding location in the WRF model during 2300 UTC 7 October and 0000 UTC 8 October. The observation data are plotted with one-minute interval. The wind observations are conducted at the top of a building and at the 35-m height from the ground surface, while the WRF winds are those at the 10-m height as a representative of the surface winds. The WRF winds generally agree well with, but are a little stronger than, the observations. Note that the WRF winds increased with height and those at the 35-m height were about two times stronger than the observed mean winds, suggesting that the WRF model cannot reproduce urban-canopy flows. Although the LES averaged values overestimate the observed mean winds during 2300 and 2340 UTC 7 October, the discrepancy between the simulation and the observation is generally within 10 %.

Figure 4 compares the time series of the instantaneous wind speeds of the LES and observation. The LES winds are those obtained at the 35-m height at the observation location, and their instantaneous values are indicated as

running-means for 3 seconds. Although the large gusty winds at 2338 UTC 7 October are not captured by the LES, the instantaneous LES winds generally vary within the range of the observed maximum instantaneous values.

In order to evaluate the performance of the LES, gust factors from the LES are compared with the observed values. The gust factor is computed as the ratio of the maximum instantaneous wind speeds for every one minute against the 10-min mean. Figure 5 compares the frequency distributions of gust factors of the LES with the observation. There are some differences between the LES and the observation. First, the gust factor at the peak frequency of the LES is different from that of the observation. Second, the frequency of the large gust factors greater than 2.0 of the LES is underestimated. These differences may be partly due to the fact that the fluctuations simulated in the WRF model, in spite of the high-frequency outputs, have smaller variations than those observed (Fig. 3). If larger fluctuations, which should be present in the real settings, could be simulated in the WRF model, gust factors represented in the LES would be enhanced. Although some differences are observed between the LES model and the observation, the frequency distribution obtained
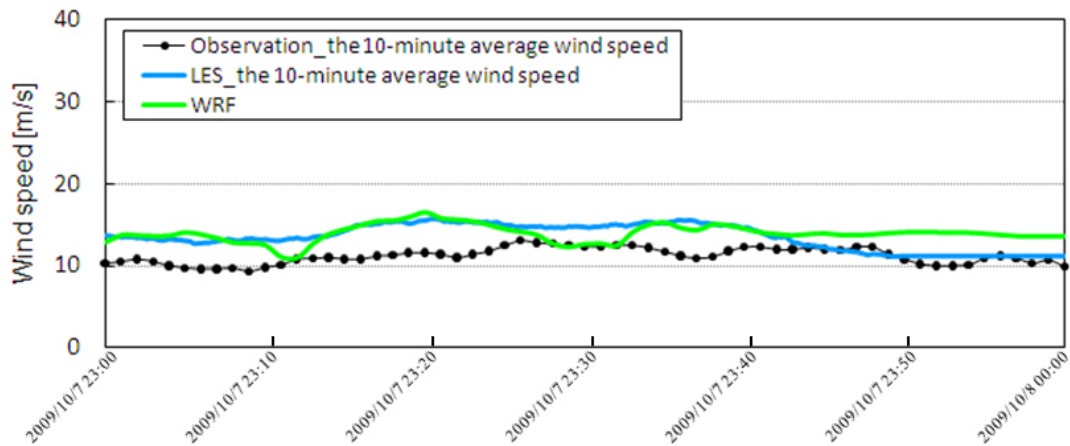
Figure 3: Time series of the horizontal wind speeds of the 10-min means (black line) at the JMA observation site (the circle point in Fig. 1f), the WRF simulation obtained at the 10-m height (green line), and the 10-min averaged values from the LES obtained at the 35-m height (blue line) during the period between 2300 UTC 7 October and 0000 UTC 8 October.
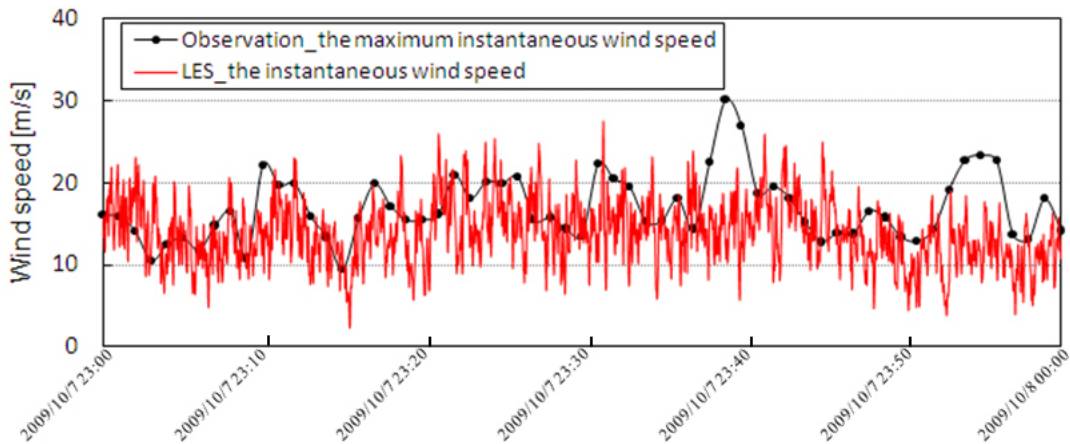
Figure 4: Time series of the horizontal wind speeds of the maximum instantaneous values (black line) at the JMA observation site (the circle point in Fig. 1f), the instantaneous (red line) values from the LES obtained at the 35-m height during the period between 2300 UTC 7 October and 0000 UTC 8 October.
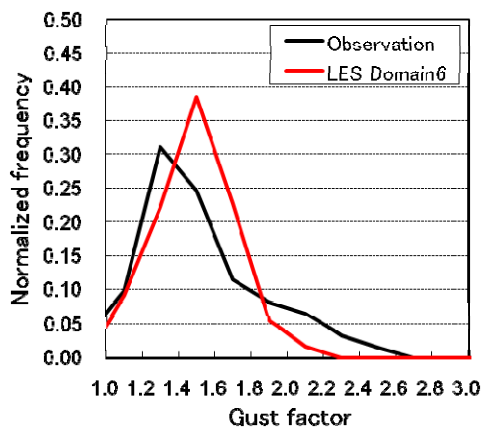
Figure 5: Normalized frequency distribution of gust factors from the observation (black line) and the LES (red line).

from the LES is generally similar to that from the observation.

The point stressed at this point is that the building effects are a significant contributor in determining the gust factors within the urban canopy.

4. CONCLUSION

The existing turbulent inflow techniques was extended to couple between NWP and CFD models and predict a strong wind event over the central district of Tokyo during the passage of Typhoon Melor (2009). The present approach was used to conduct an LES of turbulent flows around

urban buildings in a real meteorological setting.

First, urban boundary layer flow from the WRF outputs was well reproduced over the LES domain where the urban surface geometries (grid resolution: 20m) are explicitly resolved. Then, this time-dependent boundary layer flow is imposed at the inflow boundary of the LES model where individual urban buildings (grid resolution: 5m) are explicitly resolved. It is found that significant decelerations of wind speeds within the urban canopy layer were reasonably represented in the LES by resolving the urban surface geometry. The ranges of wind fluctuations and gust factors were also found to be well reproduced in the LES. From these results, it is considered that the present approach to couple an LES model with a NWP model and predict gusty winds over urban areas should be effective.

REFERENCES

Chorin, A. J., 1967: A numerical method for solving incompressible viscous flow problems. *Journal of Computational Physics*, **2**, 12-26.

Goldstein, D., R. Handler, and L. Sirovich, 1993: Modeling a no-slip flow boundary with an external force field. *Journal of Computational Physics*, **105**, 354-366.

Gresho, P. M., 1992: Some interesting issues in incompressible fluid dynamics, both in the continuum and in numerical simulation. *Advances in Applied Mechanics*, **28**, 45–140.

Janjic, Z. I., 2002: Nonsingular implementation of the Mellor-Yamada level 2.5 scheme in the NCEP Meso model. *NCEP Office Note*, **437**, 61 pp.

Lund T. S., X. Wu, and K. D. Squires, 1998: Generation of turbulent inflow data for spatially-developing boundary layer simulations. *Journal of Computational Physics*, **140**, 233-258.

Nakayama, H., T. Takemi, and H. Nagai, 2011: LES analysis of the aerodynamic surface properties for turbulent flows over building arrays with various geometries. *Journal of Applied Meteorology and Climatology*, **50**, 8, 1692-1712.

Skamarock, W. C., Klemp, J. B., Dudhia, J., Gill, D. O., Barker, D. M., Duda, M. G., Huang, X.-Y., Wang, W., Powers, J. G., 2008. A description of the Advanced Research WRF Version 3, *NCAR Tech. Note*, **NCAR/TN-475+STR**, 1 pp.

Smagorinsky J. 1963. General circulation experiments with the primitive equations. *Monthly Weather Review*, **91**, 99-164.

Van der Hoven. 1957. Power spectrum of horizontal wind speed in the frequency range from 0.0007 to 900 cycles per hour. *Journal of Meteorology*, **14**, 2, 160-164.